believe, therefore, that the observed temperature shift in β-brass is the first relevant experimental evidence for the predictions of Fisher and Burford.

I am grateful to M. E. Fisher and A. R. Mackintosh for discussions on the interpretation of the reported experimental results, and to L. Passell of Brookhaven National Laboratory for help in procuring the separated Cu^{65} used in the crystal.

PHYSICAL REVIEW VOLUME 185, NUMBER 2 10 SEPTEMBER 1969

Nernst Effect and Flux Flow in Superconductors. III. Films of Tin and Indium*

V. A. Rowe and R. P. Huebener
Argonne National Laboratory, Argonne, Illinois 60439
(Received 21 April 1969)

Flux motion induced by a temperature gradient and by an electrical current has been studied through the Nernst effect and the flux-flow resistivity in superconducting films of tin and indium. The film thickness ranged between 1 and 11 μm for tin and between 0.5 and 5 μm for indium. The data were taken at 2.0 K as a function of magnetic field and film thickness. In addition to the transport entropy of a fluxoid and the flux-flow resistivity, the critical thermal force and the critical Lorentz force, at which thermally induced and current-induced flux motion sets in, were determined. The transport entropy per unit length per unit flux, S_φ/φ, plotted versus film thickness was found to reach a maximum in Sn at about 7 μm and in In at about 3.5 μm. Around this maximum, S_φ/φ was larger by a factor of 1.4 in Sn and 1.6 in In than the value calculated from the difference in entropy density of normal and superconducting material. With increasing film thickness, the critical Lorentz force decreased, while the critical thermal force increased. The discrepancy between the critical Lorentz force and the critical thermal force and its dependence on film thickness suggests that in the films the critical current flows along special channels at the surface for which the interaction with the fluxoids is strongly reduced. The results on Sn and In are consistent with the earlier results on Pb.

I. INTRODUCTION

RECENTLY we reported measurements of the Nernst effect in the mixed state of superconducting niobium[1] and in the intermediate state of superconducting lead films.[2] In this paper we present the results of an extension of these measurements to superconducting films of tin and indium. The results obtained are similar to those reported in II for lead.

A summary of the theory and the scheme used for the analysis of the data can be found in I. Some of the experimental techniques described in I and II have been modified for the present work. Those parts of the experimental procedures which have been modified are described in Sec. II.

II. EXPERIMENTAL

The samples for these experiments were prepared by vacuum deposition of 99.9999% pure material[3] on 1-mm-thick microscope slides that had been cut to $1\frac{1}{2}\times\frac{13}{16}$ in. to fit the cryostat. The starting pressure in the bell jar was $\sim 5\times 10^{-8}$ Torr. During evaporation the pressure was in the 10^{-6}-Torr range for all samples except In 24 and In 26, for which the pressures were each an order of magnitude higher. The distance between the joule-heated tantalum boat and the sample substrates was 31 cm. With the exception of the two mentioned above, all samples were masked by a copper foil prepared by a photographic-reduction-and-etching process, thus giving a relative precision of sample dimensions of about $\frac{1}{2}$%. Substrates were cleaned first in detergent, then in an ultrasonic cleaner and finally in a vapor degreaser operating with trichloroethylene.

Film thickness d was measured routinely by the weight and the electrical resistance and checked occasionally by multiple-beam interferometry. The three methods were in good agreement for all the samples. Table I shows dimensions and residual-resistance ratios ($RRR=R_{295}/R_{4.2}$) of all the films except the In films of thickness greater than 3 μm, where the Nernst voltages were negligibly small. The sample configuration is shown schematically in Fig. 1. Number 36 Teflon insulated niobium lead wires were soldered to

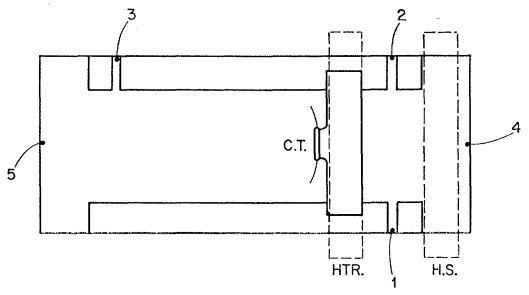

FIG. 1. Specimen geometry, including the heater (HTR), heat sink (HS), carbon thermometer (CT), Nernst probes (1 and 2) longitudinal voltage probes (2 and 3), and current leads (4 and 5).

* Based on work performed under the auspices of the U. S. Atomic Energy Commission.
[1] R. P. Huebener and A. Seher, Phys. Rev. 181, 701 (1969) (hereafter referred to as I).
[2] R. P. Huebener and A. Seher, Phys. Rev. 181, 710 (1969) (hereafter referred to as II).
[3] Source: Semi-Elements, Inc., Saxonburg, Pa. 16056.

TABLE I. Sample details.

	In24	In26	In45	In47	Sn25	Sn27	Sn35	Sn39	Sn41
$d(\mu m)$	0.5	1.0	2.0	2.9	1.0	2.1	3.4	6.2	11.0
l_1 (cm)[a]	0.5	0.6	0.3	0.3	0.3	0.3	0.3	0.3	0.3
l_2 (cm)[a]	1.8	1.8	2.0	2.0	2.0	2.0	2.0	2.0	2.0
w (cm)[a]	1.3	1.25	1.2	1.2	1.2	1.2	1.2	1.2	1.2
R.R.R.	72	137	287	390	83	119	212	300	324
H(Oe)	74	76	80	84	128	128	128	128	128
∇T_c(K/cm)	0.10	0.15	0.50	0.57	0.40	0.33	0.22	0.18	0.27
I_c(mA)	2.6	2.2	16.2	5.7	7.9	12.0	5.8	8.0	7.2
J_c(A/cm^2)	58	18	68	16	66	48	14	10	5

[a] l_1 is the distance between heater and heat sink; l_2 is the distance between longitudinal voltage probes; and w is the width of film and distance between Nernst probes.

the substrate with pure indium in the appropriate positions prior to the deposition. Since the niobium wires were always superconducting in these experiments, no spurious thermal emf's could be generated in them. Furthermore, their heat conductivity was small, thus reducing errors that might be produced by large heat currents flowing to or from the sample.

The pressure over the helium bath was stabilized with a Walker type manostat and measured with a Texas Instruments quartz Bourden gauge. This procedure enabled us to hold the bath temperature within a few millidegrees for periods of several hours.

Flux-flow resistance measurements were taken isothermally at 2.0 K with 100–200 microns of He exchange gas in the cryostat, while Nernst data were recorded with a good ($<10^{-5}$ Torr, measured at room temperature) vacuum inside. The temperature at the noninductively wound heater was measured using a 100 Ω, 1/10 W Allen Bradley carbon resistor epoxied with Stycast 2850 GT to a Cu foil. The foil-resistor assembly was clamped between the heater and the film using Apiezon grade-N grease (see Fig. 1). Considerable care was taken to see that the Nernst probes 1 and 2 were centered between the heater and the heat sink. Thus a constant temperature could be held at the Nernst probes while establishing a temperature gradient

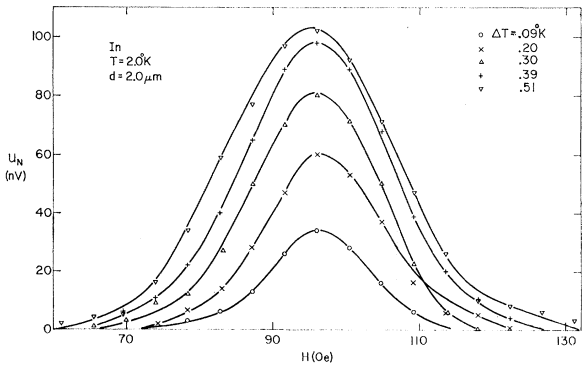

FIG. 2. Nernst voltages U_N plotted versus magnetic field H for a 2-μm In film for the temperature differences between heater and heat sink indicated.

by pumping the bath down in temperature and, at the same time, passing current through the heater.

The resistance of the carbon thermometer was measured using an ac Wheatstone bridge with a Gertsch ratio transformer as the variable leg and a P.A.R. model HR-8 lock-in amplifier as the detector and current source. This arrangement allowed submillidegree temperature resolution while dissipating less than 10^{-11} watts in the thermometer. It was found that the epoxy encapsulation of the carbon resistance element reduced calibration shifts markedly. Calibrations were made at intervals of several months against the T_{58} scale and found to be reproducible to within about 2 mdeg.

III. RESULTS

Figure 2 shows some results obtained for Nernst voltages taken with varying magnetic field for different temperature gradients. In both materials, the magnetic-field value at which the peak voltage occurs varies in position with thickness. The degree of symmetry of the curves about the peak value seemed to depend on the accuracy of sample alignment and temperature control at the heater and heat sink.

Figure 3 is an example of data derived from curves like those in Fig. 2. This clearly shows the linear dependence of the Nernst effect on temperature gradient.

The Nernst effect was found to be too small to be measurable for films of In thinner than 0.5 μm and thicker than 3 μm. The same was true of Sn films below 1 μm, but no upper limit has been reached, although the effect is diminished in the thickest film measured ($d=11$ μm).

Typical resistance data are shown in Fig. 4. Here again a linear region appears whose slope we take to be equal to the flux-flow resistance. The resistive transition is found to be spread over a wide range of magnetic field.

Table I shows critical-temperature gradients, critical currents, and critical-current densities for the samples at the magnetic-field values indicated. The critical

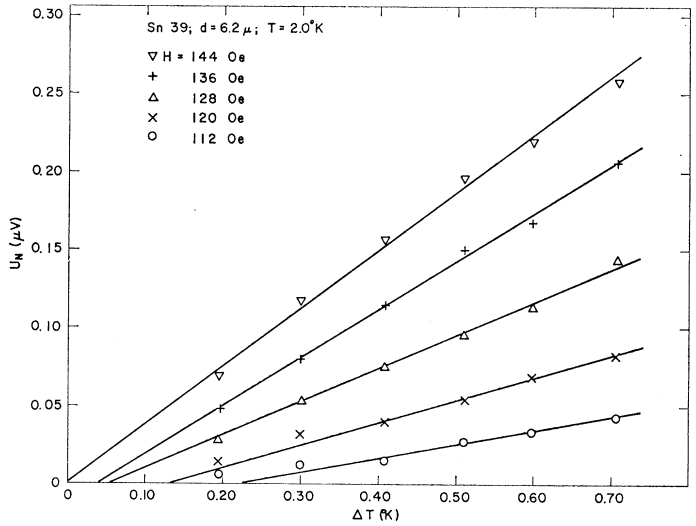

FIG. 3. Nernst voltages U_N plotted versus temperature difference at the magnetic field values listed for a 6.2-μm Sn film.

values are determined by linear extrapolation of the linear portions of curves like those shown in Fig. 3 and 4 to zero Nernst and resistive voltage.

While the critical currents behave in an understandable way, proceeding monotonically to zero as the magnetic field is raised, the critical temperature gradients show a small region of negative values in the vicinity of the peak of the Nernst voltage. The measured critical currents show little correlation with film thickness and the variations present may be due to differences in deposition rate, vacuum during deposition, and similar metallurgical effects. The critical-temperature gradient in Sn depends on d much as was observed in Pb, while the variation in In appears to be somewhat different.

From the electrical resistance and film thickness measurements, it is possible to extract the bulk resistivity and the electron-mean-free path. Assuming diffuse surface scattering, the difference in resistivity, $\Delta\rho$, between a bulk specimen of mean free path l_0 and resistivity ρ_0 and a film of thickness d is[4]

$$\Delta\rho = (3l_0/8d)\rho_0. \quad (1)$$

Assuming Matthiessen's rule for the surface scattering, $\Delta\rho$ may be expressed[5] in terms of the bulk resistance ratio B, and the film resistance ratio A, where A and B are taken between 295 and 4°K:

$$\Delta\rho = \rho_0(295°\text{K}) \times [(1-A/B)/(A-1)]. \quad (2)$$

Combining (1) and (2) we find

$$(A-1)/(1-A/B) = (8/3l_0)d \quad (3)$$

Figure 5 is a plot of the expression in the left-hand side of Eq. (3) versus film thickness for all the samples studied during the course of the present experiments. In the case of In, the bulk ratio B, of 2.25×10^4 measured on a $\frac{1}{2}\times1$ in. rod gives a good fit. For Sn however, B had to be adjusted to an apparent value of 639 in order to obtain a straight line passing through the origin. This is probably related to the well-known difficulties of preparing "clean" Sn films. From the slopes of the lines in Fig. 5 and from measured values of $\rho_0(295°\text{K})$ of 8.54 μΩ cm for In and 11.2 μΩ cm for Sn, we calculate $\rho_0 l_0$ values of 1.65×10^{-11} and 3.25×10^{-11} Ω cm² for In and Sn, respectively. At least in the case of Sn it should be recognized that the slope is dependent on the value of B used, and may vary by a factor of 2 for reasonable choices of this parameter. Our measured resistivities compare well with $\rho_0(295°\text{K})$

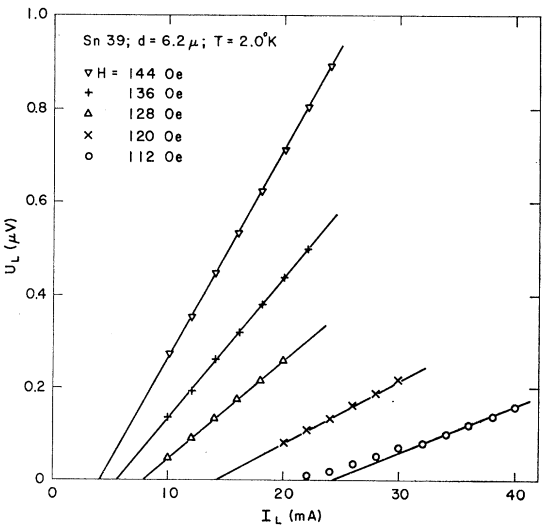

FIG. 4. Resistive voltages U_L shown as a function of longitudinal current I_L for a 6.2-μm Sn film at the magnetic field values indicated.

[4] E. H. Sondheimer, Advan. Phys. **1**, 1 (1952).
[5] R. P. Huebener, Phys. Rev. **136**, A1740 (1964).

values quoted by Meaden[6]: 8.7 $\mu\Omega$ cm for In and 11.0 $\mu\Omega$ cm for Sn.

The data presented in this section allow the construction of profiles of the transport entropy per unit length per unit flux, S_φ/φ, versus magnetic field H, and film thickness d, according to the two schemes presented in Eqs. (9) and (11) of I.

The first method to be considered [Eq. (9) of I] makes use of the linear regions in the Nernst voltage versus ∇T and flux-flow curves. We note that the values of S_φ/φ derived from Eq. (6) in II are 7.1 Oe/K for Sn and 7.6 Oe/K for In. Figure 6 is a composite profile of the magnetic field and thickness dependence of S_φ/φ in Sn. The same is shown for In in Fig. 7.

The second method of calculating the transport entropy [Eq. (11) of I] involves setting the critical thermal and Lorentz force equal to one another. The entropy values obtained in this way are significantly larger than those obtained using the previous method, as has already been observed in I and II. In Fig. 8 the ratio D,

$$D=\frac{|J_c/\nabla T_c|}{S_1/S_2}, \tag{4}$$

is plotted for both materials as a function of film thickness at the magnetic field values listed in Table I. Here J_c and ∇T_c are the critical-current density and the critical-temperature gradient, respectively. S_1/S_2 is the ratio of the slopes defined in Eqs. (5) and (8) of I. We see that D approaches unity in very thick films and increases with decreasing film thickness. As a function of film thickness we plot in Fig. 9 the product $(S_1/S_2)\nabla T_c$ which is the critical thermal force per flux and per unit length.

IV. DISCUSSION

A. Transport Entropy

The transport entropy of the fluxoids in tin and indium is found to have a dependence on magnetic field and film thickness similar to that reported in II for lead. S_φ/φ approaches zero as the magnetic field nears the critical field. Very thin and very thick films show only small values of the transport entropy, while at some intermediate thickness the transport entropy reaches a maximum.

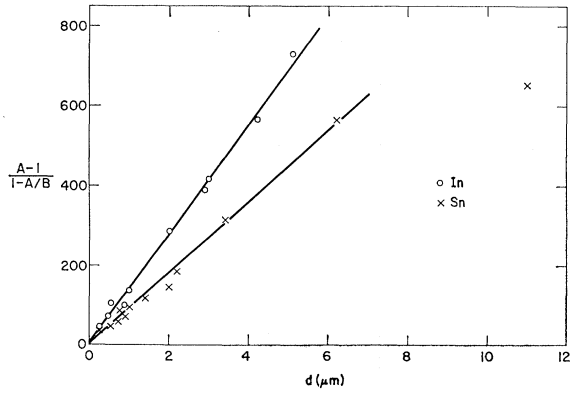

FIG. 5. Plot of the ratio defined in Eq. (3) of the text versus film thickness d for all the samples.

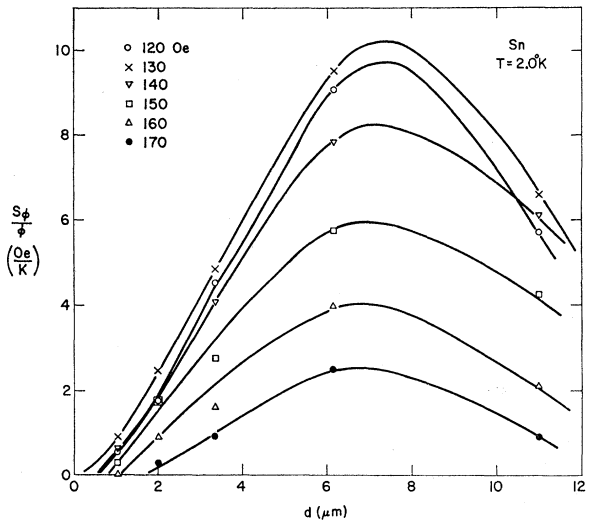

FIG. 6. The transport entropy per flux, S_φ/φ, plotted versus film thickness d at various magnetic field values for the Sn films at 2°K.

To understand the dependence of S_φ/φ on magnetic field and film thickness we use the same arguments as in II. As we approach the critical field the normal regions become larger and larger and therefore less and less localized. For very thin films, the distance between individual fluxoids may be so small that there is some interaction between neighboring fluxoids resulting in a reduced localization of the normal fluxoid cores. With increasing film thickness the fluxoids are more localized, because (for constant magnetic field) the fluxoid size and the distance between the fluxoids become larger. As the film thickness increases further, the larger and larger normal regions become less and less mobile. As will be discussed in Sec. IV B, the critical thermal force per flux and per unit length of fluxoid increases with increasing film thickness, indicating stronger pinning of the flux structure in the very thick films. If the large normal patches stretch across the width of the sample during the flux-flow resistance measurements, the resistive voltage will be only partly due to flux flow and partly to Ohmic losses. In this case the slope S_2 will be larger than the value corresponding to the flux motion and will result in a diminished apparent-transport entropy.

In II it was suggested that the decrease of S_φ/φ with decreasing film thickness should be reduced as the magnetic field is lowered. The data in Fig. 6 indicate such behavior, thus supporting the model proposed in II and used above. From Figs. 6 and 7 we note that

[6] G. T. Meaden, *Electrical Resistance of Metals* (Plenum Press, Inc., New York, 1965), p. 17.

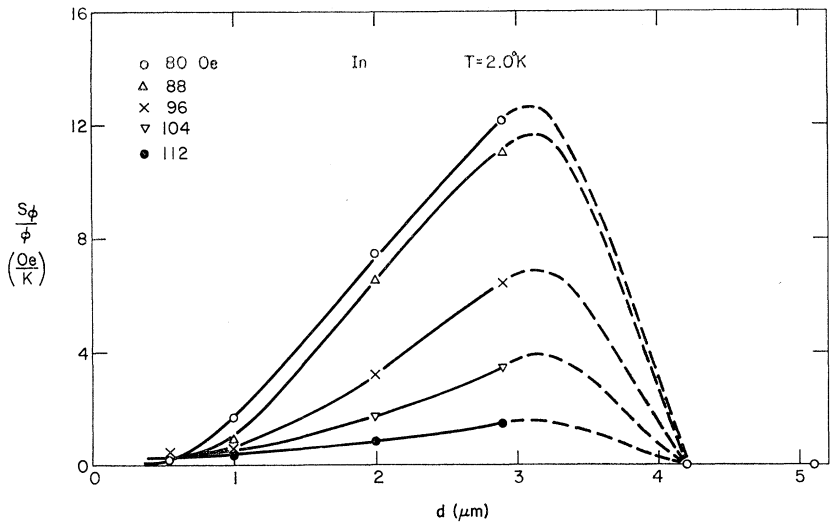

FIG. 7. The transport entropy per flux S_φ/φ plotted versus film thickness d at the magnetic field values indicated for the In films at 2 K.

around its maximum S_φ/φ is larger than the calculated value from Eq. (6) in II by as much as a factor of 1.4 in Sn and 1.6 in In. The expression given in Eq. (6) of II has been obtained for a very large flux bundle, in which the contribution of the surface between normal and superconducting material can be neglected. The fact that Sn and In films show values of S_φ/φ which are larger than the value given by Eq. (6) of II suggests that in these specimens the surface energy contributes appreciably to the transport entropy of a fluxoid.

The model we used to explain the increase of S_φ/φ with increasing film thickness predicts that this increase should be stronger in In than in Sn because of the higher surface energy in In.[7] The data are consistent with this conclusion.

B. Critical Current and Critical-Temperature Gradient

The results on the critical current and the critical-temperature gradient and the conclusions drawn from them are very similar to those reported in II for lead. From the fact that for small film thickness the ratio D is much larger than unity, we conclude that at and below its critical value, the current flows through special channels in the specimen in such a way that the Lorentz force is much smaller than the value found from the average current density (total current divided by sample cross section) in the sample. The fact that D is larger than unity and increases with decreasing film thickness suggests that these current channels are associated with the specimen surface. This model may be summarized as follows: The current flows initially with inhomogeneous density, avoiding the flux bundles. Since the current density within the flux bundles is zero, there will be no Lorentz force. As the current becomes larger, more current flows through the flux bundles, thus leading to a finite Lorentz force. Finally the current flows along the sample with uniform density thus producing the full Lorentz force and establishing the linear–flux-flow region. This also suggests an explanation for the curvature in the voltage-current curves below the linear region in terms of a gradual increase of the interaction between the total current and the flux structure. This mechanism is quite different from that considered in the past for explaining the curved region in the voltage-current curves, which involved inhomogeneities in the flux pinning property of the specimens. We note that the present mechanism results in a finite critical current (obtained by extrapolating the linear branch in the voltage-current curves linearly to zero voltage) even without flux pinning.

In Table I it may be seen that the critical current does not vary in any consistent way with film thickness. From the independence of the critical current of the specimen thickness, and thereby of the fluxoid size,

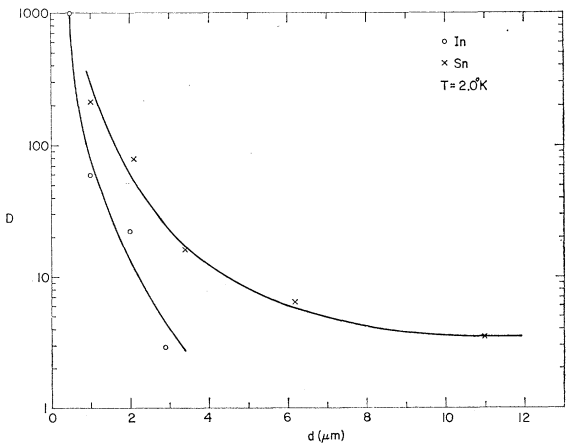

FIG. 8. The ratio D, as defined in Eq. (4) of the text, plotted versus film thickness for both In and Sn at 2 K.

[7] E. A. Davies, Proc. Roy. Soc. (London) **A255**, 407 (1960).

we may conclude that the critical current depends only on the total area occupied by the normal flux-tube cores and not on its distribution. Increasing the magnetic field increases the relative area occupied by the normal regions and decreases the area available to subcritical currents. Thus we see a steady decrease of the critical current with increasing magnetic field. We emphasize that in our discussion of the critical current no flux pinning mechanism has been involved.

In the following we discuss the behavior of the critical thermal force with some simple assumptions about flux pinning. In order to understand the increase of $(S_1/S_2)(\partial T/\partial x)_c$, that is of the critical thermal force per flux and per unit length, with increasing film thickness (Fig. 9), we assume that a spectrum of pinning centers with differing strengths exists in the specimens and that the average pinning center concentration is independent of film thickness. In a thick film with few but rather large flux bundles the fluxoids will be pinned predominantly at those sites with the strongest pinning force. As the film thickness becomes smaller (at constant magnetic field), more and more fluxoids of smaller and smaller size exist and will be pinned at the sites with smaller pinning forces. This rather *ad-hoc* picture then gives the correct dependence of the critical thermal force on thickness consistent with the model proposed.

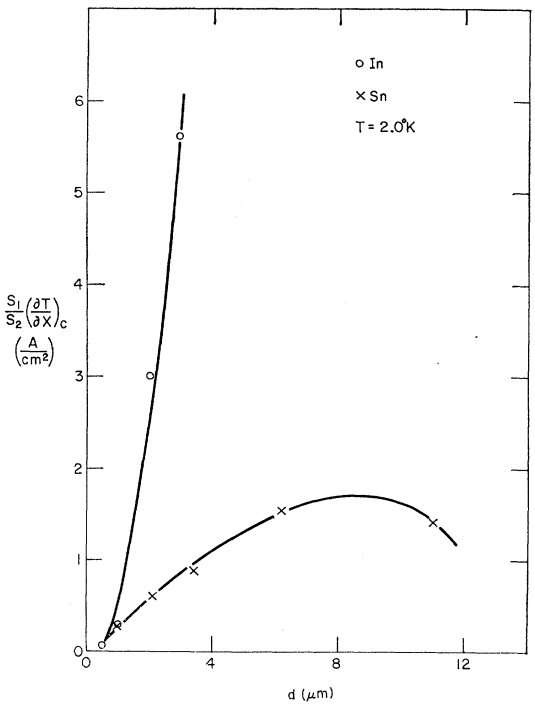

FIG. 9. The critical thermal force per flux and per unit length, $(S_1/S_2)(\partial T/\partial x)_c$, plotted against film thickness at 2°K for In ($H \approx 80$ Oe) and Sn ($H = 128$ Oe).

V. SUMMARY

The transport entropy in thin films of tin and indium and its dependence on film thickness and magnetic field has been measured through the Nernst effect. The dependence of the transport entropy on magnetic field and film thickness can be qualitatively understood and is consistent with the results on lead reported in II. In the films, the critical Lorentz force is always larger than the critical thermal force, the discrepancy increasing strongly with decreasing film thickness. This suggests that the critical current flows along special channels at the surface for which the interaction with the fluxoids is strongly reduced, in agreement with the earlier results on lead. An attempt has been made to understand the behavior of the critical current and critical thermal force in terms of a simple model for the flux bundles and pinning centers.

ACKNOWLEDGMENT

The authors wish to thank B. Bryson for his assistance in preparing the samples and taking data.